# Design of Self-supporting Surfaces

Etienne Vouga
Columbia Univ. / KAUST

Mathias Höbinger
Evolute / TU Wien

Johannes Wallner
TU Graz / TU Wien

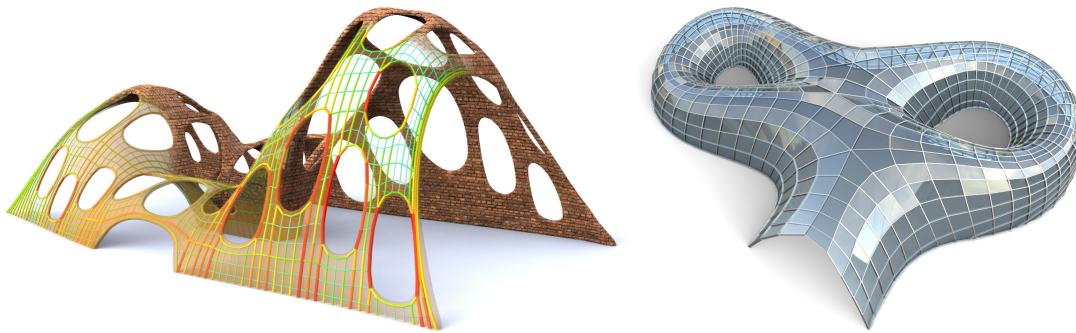Helmut Pottmann
KAUST

**Figure 1:** Left: *Surfaces with irregularly placed holes are hard to realize as masonry, where the mortar between bricks must not be subject to tensile stresses. The surface shown here, surprisingly, has this property – it has been found as the nearest self-supporting shape from a given freeform geometry. The fictitious thrust network used in our algorithms is superimposed, with edges' cross-section and coloring visualizing the magnitude of forces (warmer colors represent higher stresses.)* Right: *Curvature analysis with respect to the Airy stress surface tells us how to remesh shapes by self-supporting quad meshes with planar faces. This guides steel/glass constructions with low moments in nodes.*

## Abstract

Self-supporting masonry is one of the most ancient and elegant techniques for building curved shapes. Because of the very geometric nature of their failure, analyzing and modeling such strutures is more a geometry processing problem than one of classical continuum mechanics. This paper uses the thrust network method of analysis and presents an iterative nonlinear optimization algorithm for efficiently approximating freeform shapes by self-supporting ones. The rich geometry of thrust networks leads us to close connections between diverse topics in discrete differential geometry, such as a finite-element discretization of the Airy stress potential, perfect graph Laplacians, and computing admissible loads via curvatures of polyhedral surfaces. This geometric viewpoint allows us, in particular, to remesh self-supporting shapes by self-supporting quad meshes with planar faces, and leads to another application of the theory: steel/glass constructions with low moments in nodes.

**CR Categories:** I.3.5 [Computer Graphics]: Computational Geometry and Object Modeling—Curve, surface, solid, and object representations;

**Keywords:** Discrete differential geometry, architectural geometry, self-supporting masonry, thrust networks, reciprocal force diagrams, discrete Laplacians, isotropic geometry, mean curvature

**Links:** DL PDF

## 1 Introduction

Vaulted masonry structures are among the simplest and at the same time most elegant solutions for creating curved shapes in building construction. For this reason they have been an object of interest since antiquity; large, non-convex examples of such structures include gothic cathedrals. They continue to be an active topic of research today.

Our paper is concerned with a combined geometry+statics analysis of *self-supporting* masonry and with tools for the interactive modeling of freeform self-supporting structures. Here "self-supporting" means that the structure, considered as an arrangement of blocks (bricks, stones), holds together by itself, with additional support present only during construction. This analysis is based on the following assumptions, which follow the classic [Heyman 1966]:

*Assumption 1:* Masonry has no tensile strength, but the individual building blocks do not slip against each other (because of friction or mortar). On the other hand, their compressive strength is sufficiently high so that failure of the structure is by a sudden change in geometry and not by material failure.

*Assumption 2 (The Safe Theorem)*: If a system of forces can be found which is in equilibrium with the load on the structure and which is contained within the masonry envelope then the structure will carry the loads, although the actual forces present may not be those postulated by that system.

Our approach is twofold: We first give an overview of the continuous case of a smooth surface under stress, which turns out to be governed locally by the Airy stress function. This mathematical model is called a membrane in the engineering literature and has been applied to the analysis of masonry before. The surface is self-supporting if and only if stresses are entirely compressive. For computational purposes, stresses are discretized as a fictitious *thrust network* [Block and Ochsendorf 2007] contained in the masonry structure; this network is a system of forces in equilibrium with the structure's deadload. It can be interpreted as a finite element discretization of the continuous case, and it turns out to have very interesting geometry, with the Airy stress function becoming a

polyhedral surface directly related to a reciprocal force diagram.

While previous work in architectural geometry was mostly concerned with aspects of rationalization and purely geometric side-conditions which occur in freeform architecture, the focus of this paper is design with *statics* constraints. In particular, our contributions are the following:

**Contributions.**  • We present an optimization algorithm, based on the theory of thrust networks and Airy potentials, for efficiently finding a self-supporting surface near a given arbitrary reference surface (§3), and build a tool for interactive design of self-supporting surfaces based on this algorithm (§4). Freeform masonry is based on such surfaces.

• The discrete "stress Laplacian" derived from a thrust network with compressive forces is a so-called perfect one (§2.2). We use it to argue why our discretizations are faithful to the continuous case.

• We connect the physics of self-supporting surfaces with the geometry of isotropic 3-space, and express the equations governing self-supporting surfaces in terms of curvatures (§2.3) and (§2.4). Likewise we establish a connection between the stress Laplacian and mean curvatures of polyhedral surfaces. This theoretical part of the paper is a contribution to Discrete Differential Geometry.

• We use the geometric knowledge we have gathered to find particularly nice families of self-supporting surfaces, especially planar quadrilateral representations of thrust networks (§5). This leads to steel/glass structures with low bending and torsion moments.

**Related Work.**  Unsupported masonry has been an active topic of research in the engineering community. The foundations for the modern approach were laid by Jacques Heyman [1966] and are available as the textbook [Heyman 1995]. The theory of reciprocal force diagrams in the planar case was studied by J. Maxwell; a unifying view on polyhedral surfaces, compressive forces and corresponding "convex" force diagrams is presented by [Ash et al. 1988]. F. Fraternali [2002; 2010] established a connection between the continuous theory of stresses in membranes and the discrete theory of forces in thrust networks, by interpreting the latter as a non-conforming finite element discretization of the former.

Several authors have studied the problem of finding discrete compressive force networks contained within the boundary of masonry structures; previous work in this area includes [O'Dwyer 1998] and [Andreu et al. 2007]. Fraternali [2010] proposed solving for the structure's discrete stress surface, and examining its convex hull to study the structure's stability and susceptibility to cracking. This approach works well for analyzing existing structures, where the boundary tractions can be measured and the stress surface is known to be close to convex, but is not an ideal design tool since in such settings the boundary tractions are unknown, and where replacing a non-convex intial stress surface by its convex hull can cause large, uncontrolled global changes to the surface being designed.

Philippe Block's seminal thesis introduced *Thrust Network Analysis*, which pioneered the use of thrust networks and their reciprocal diagrams for efficient and practical design of self-supporting masonry structures. By first seeking a reciprocal diagram of the top view, guaranteeing equilibrium of horizontal forces, then solving for the heights that balance the vertical loads, Thrust Network Analysis linearizes the form-finding problem. For a thorough overview of this methodology, see e.g. [Block and Ochsendorf 2007; Block 2009]. Recent work by Block and coauthors extends this method in the case where the reciprocal diagram is not unique; for different choices of reciprocal diagram, the optimal heights can be found using the method of least squares [Van Mele and Block 2011], and the

search for the best such reciprocal diagram can be automated using a genetic algorithm [Block and Lachauer 2011].

Other approaches to the design of self-supporting structures include modeling these structures as damped particle-spring systems ("dynamic relaxation" methods) [Kilian and Ochsendorf 2005; Barnes 2009], and mirroring the rich tradition in architecture of designing self-supporting surfaces using hanging chain or membrane models (for instance by Frei Otto, Antoni Gaudi, and Heinz Isler) [Heyman 1998; Kotnik and Weinstock 2012]. Force density methods [Linkwitz and Schek 1971] linearize the form-finding problem by solving for static equilibrium with respect to position variables, given prescribed prestresses in the form of axial force densities [Gründig et al. 2000]. Alternatively, masonry structures can be represented by networks of rigid blocks [Livesley 1992], whose conditions on the structural feasibility were incorporated into procedural modeling of buildings [Whiting et al. 2009].

Algorithmic and mathematical methods relevant to this paper are work on the geometry of PQ meshes [Liu et al. 2006], discrete curvatures for such meshes [Pottmann et al. 2007; Bobenko et al. 2010], in particular curvatures in isotropic geometry [Pottmann and Liu 2007]. Schiftner and Balzer [2010] discuss approximating a reference surface by a quad mesh with planar faces, whose layout is guided by statics properties of that surface.

## 2  Self-supporting Surfaces

This section contains the theoretical basis of the paper. We begin in §2.1 and §2.2 with a review of the continuous theory of self-supporting surfaces, and their discretization as thrust networks [Block and Ochsendorf 2007]. This discrete model and its associated equilibrium equations form the groundwork of our optimization algorithm (§4) for designing self-supporting surfaces. In §2.3, §2.4, and §2.5 we draw connections between the theory of self-supporting surfaces, curvature measures in isotropic geometry, and discrete Laplace-Beltrami operators. These insights lead to some observations on existence of convergence of discrete approximations to smooth self-supporting surfaces, and are important for the later discussions of planar quad remeshing and special classes of self-supporting surfaces (§5).

### 2.1  The Continuous Theory

We model masonry as a surface given by a height field $s(x, y)$ defined in some planar domain $\Omega$. We assume a vertical load density $F(x, y)$ over the top view — usually $F$ represents the structure's own weight. By definition this surface is self-supporting if and only if there exists a negative semidefinite (compressive) stress tensor $\sigma$ over the surface whose stresses are in equilibrium with the acting forces. Rewriting the equilibrium equations in plane coordinates $(x, y)$, we have that such a stress tensor exists if and only if there exists a field $M(x, y) = -\sigma g^{-1} \det g$ of $2 \times 2$ symmetric positive semidefinite matrices satisfying

$$\operatorname{div}(M \nabla s) = F, \quad \operatorname{div} M = 0, \tag{1}$$

where $g$ is the induced metric $\begin{pmatrix} 1+s_x^2 & s_x s_y \\ s_x s_y & 1+s_y^2 \end{pmatrix}$ and the divergence operator $\operatorname{div} \begin{pmatrix} u(x,y) \\ v(x,y) \end{pmatrix} = u_x + v_y$ is understood to act on the columns of a matrix (see e.g. [Fraternali 2010], [Giaquinta and Giusti 1985]).

The condition $\operatorname{div} M = 0$ says that $M$ is locally the Hessian of a real-valued function $\phi$ (the *Airy stress potential*) [Green and Zerna 2002]: With the notation

$$M = \begin{pmatrix} m_{11} & m_{12} \\ m_{12} & m_{22} \end{pmatrix} \iff \widehat{M} = \begin{pmatrix} m_{22} & -m_{12} \\ -m_{12} & m_{11} \end{pmatrix}$$
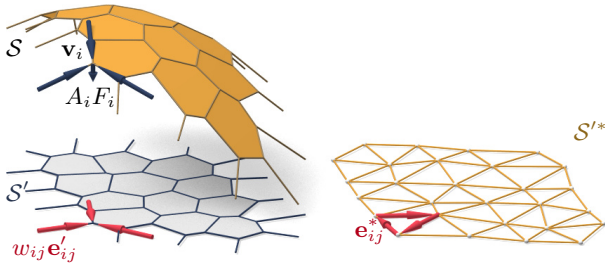
**Figure 2:** *A thrust network $\mathcal{S}$ with dangling edges indicating external forces (left). This network together with compressive forces which balance vertical loads $A_i F_i$ projects onto a planar mesh $\mathcal{S}'$ with equilibrium compressive forces $w_{ij}\mathbf{e}'_{ij}$ in its edges. Rotating forces by $90°$ leads to the reciprocal force diagram $\mathcal{S}'^*$ (right).*

it is clear that $\operatorname{div} M = 0$ is an integrability condition for $\widehat{M}$, so locally there is a potential $\phi$ with

$$\widehat{M} = \nabla^2 \phi, \quad \text{i.e.,} \quad M = \widehat{\nabla^2 \phi}.$$

If the domain $\Omega$ is simply connected, this relation holds globally. Positive semidefiniteness of $M$ (or equivalently of $\widehat{M}$) characterizes *convexity* of the Airy potential $\phi$. The Airy function enters computations only by way of its derivatives, so global existence is not an issue.

*Remark:* Stresses at boundary points depend on the way the surface is anchored: A fixed anchor means no condition, but a free boundary with outer normal vector $\mathbf{n}$ means $\langle M\nabla s, \mathbf{n}\rangle = 0$.

**Stress Laplacian.** Note that $\operatorname{div} M = 0$ yields $\operatorname{div}(M\nabla s) = \operatorname{tr}(M\nabla^2 s)$, which we like to call $\Delta_\phi s$. The operator $\Delta_\phi$ is symmetric. It is elliptic (as a Laplace operator should be) if and only if $M$ is positive definite, i.e., $\phi$ is strictly convex. The balance condition (1) may be written as $\Delta_\phi s = F$.

## 2.2 Discrete Theory: Thrust Networks

We discretize a self-supporting surface by a mesh $\mathcal{S} = (V, E, F)$ (see Figure 2). Loads are again vertical, and following Block [2007] we discretize them as force densities $F_i$ associated with vertices $\mathbf{v}_i$. The load acting on this vertex is then given by $F_i A_i$, where $A_i$ is an area of influence (using a prime to indicate projection onto the $xy$ plane, $A_i$ is the area of the Voronoi cell of $\mathbf{v}'_i$ w.r.t. $V'$). We assume that stresses are carried by the edges of the mesh: the force exerted on the vertex $\mathbf{v}_i$ by the edge connecting $\mathbf{v}_i, \mathbf{v}_j$ is given by

$$w_{ij}(\mathbf{v}_j - \mathbf{v}_i), \quad \text{where} \quad w_{ij} = w_{ji} \geq 0.$$

The weights $w_{ij}$ in these equations can be interpreted as axial force densities along the edges. The nonnegativity of the individual weights $w_{ij}$ expresses the compressive nature of forces. The balance conditions at vertices then read as follows: With $\mathbf{v}_i = (x_i, y_i, s_i)$ we have

$$\sum\nolimits_{j\sim i} w_{ij}(x_j - x_i) = \sum\nolimits_{j\sim i} w_{ij}(y_j - y_i) = 0, \quad (2)$$

$$\sum\nolimits_{j\sim i} w_{ij}(s_j - s_i) = A_i F_i. \quad (3)$$

A mesh equipped with edge weights in this way is a discrete *thrust network* [Block 2009]. Invoking the safe theorem, we can state that a masonry structure is self-supporting, if we can find a thrust network with compressive forces which is entirely contained within the structure. In other words, for a given surface the $\mathbf{v}_i$ are known and
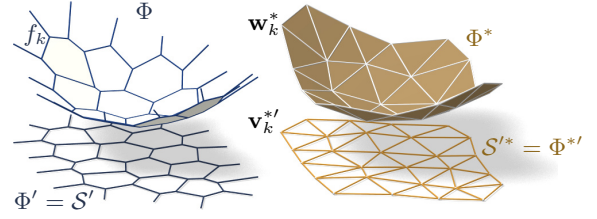


**Figure 3:** *Airy stress potential $\Phi$ and its polar dual $\Phi^*$. $\Phi$ projects onto the same planar mesh as $\mathcal{S}$ does, while $\Phi^*$ projects onto the reciprocal force diagram. A primal face $f_k$ lies in the plane $z = \alpha x + \beta y + \gamma \iff$ the corresponding dual vertex is $\mathbf{w}_k^* = (\alpha, \beta, -\gamma)$.*

the $w_{ij}$ are unknown; the surface is self-supporting whenever a solution $\{w_{ij}\}$ to the above equations exist. Finding a self-supporting surface near one that is not amounts to solving for a simultaneous solution in $\mathbf{v}_i$ and $w_{ij}$; we describe one efficient approach for doing so in §3.

**Reciprocal Diagram.** Equations (2) have a geometric interpretation: with edge vectors

$$\mathbf{e}'_{ij} = \mathbf{v}'_j - \mathbf{v}'_i = (x_j, y_j) - (x_i, y_i),$$

Equation (2) asserts that vectors $w_{ij}\mathbf{e}'_{ij}$ form a closed cycle. Rotating them by 90 degrees, we see that likewise

$$\mathbf{e}'^*_{ij} = w_{ij} J \mathbf{e}'_{ij}, \quad \text{with} \quad J = \begin{pmatrix} 0 & -1 \\ 1 & 0 \end{pmatrix},$$

form a closed cycle (see Figure 2). If the mesh $\mathcal{S}$ is simply connected, there exists an entire *reciprocal diagram* $\mathcal{S}'^*$ which is a combinatorial dual of $\mathcal{S}$, and which has edge vectors $\mathbf{e}'^*_{ij}$ [Block and Ochsendorf 2007]. Its vertices are denoted by $\mathbf{v}'^*_i$.

*Remark:* If $\mathcal{S}'$ is a Delaunay triangulation, then the corresponding Voronoi diagram is an example of a reciprocal diagram.

**Polyhedral Stress Potential.** We can go further and construct a convex polyhedral "Airy stress potential" surface $\Phi$ with vertices $\mathbf{w}_i = (x_i, y_i, \phi_i)$ combinatorially equivalent to $\mathcal{S}$ by requiring that a primal face of $\Phi$ lies in the plane $z = \alpha x + \beta y + \gamma$ if and only if $(\alpha, \beta)$ is the corresponding dual vertex of $\mathcal{S}'^*$ (see Figure 3). Obviously this condition determines $\Phi$ up to vertical translation. For existence see [Ash et al. 1988]. The inverse procedure constructs a reciprocal diagram from $\Phi$. This procedure works also if forces are not compressive: we can construct an Airy mesh $\Phi$ which has planar faces, but it will no longer be a convex polyhedron.

The vertices of $\Phi$ can be interpolated by a piecewise-linear function $\phi(x, y)$. It is easy to see that the derivative of $\phi(x, y)$ jumps by the amount $\|\mathbf{e}'^*_{ij}\| = w_{ij}\|\mathbf{e}'_{ij}\|$ when crossing over the edge $\mathbf{e}'_{ij}$ at right angle, with unit speed. This identifies $\Phi$ as the Airy polyhedron introduced by [Fraternali et al. 2002] as a finite element discretization of the continuous Airy function (see also [Fraternali 2010]).

If the mesh is not simply connected, the reciprocal diagram and the Airy polyhedron exist only locally. Our computations do not require global existence.

**Polarity.** Polarity with respect to the *Maxwell paraboloid* $z = \frac{1}{2}(x^2+y^2)$ maps the plane $z = \alpha x+\beta y+\gamma$ to the point $(\alpha, \beta, -\gamma)$. Thus, applying polarity to $\Phi$ and projecting the result $\Phi^*$ into the $xy$ plane reconstructs the reciprocal diagram $\Phi^{*\prime} = \mathcal{S}'^*$ (see Fig. 3).

**Discrete Stress Laplacian.** The weights $w_{ij}$ may be used to define a graph Laplacian $\Delta_\phi$ which on vertex-based functions acts as

$$\Delta_\phi s(\mathbf{v}_i) = \sum_{j \sim i} w_{ij}(s_j - s_i).$$

This operator is a perfect discrete Laplacian in the sense of [Wardetzky et al. 2007], since it is symmetric by construction, Equation (2) implies linear precision for the planar "top view mesh" $\mathcal{S}'$ (i.e., $\Delta_\phi f = 0$ if $f$ is a linear function), and $w_{ij} \geq 0$ ensures semidefiniteness and a maximum principle for $\Delta_\phi$-harmonic functions. Equation (3) can be written as $\Delta_\phi s = AF$.

Note that $\Delta_\phi$ is well defined even when the underlying meshes are not simply connected.

## 2.3 Surfaces in Isotropic Geometry

It is worthwhile to reconsider the basics of self-supporting surfaces in the language of dual-isotropic geometry, which takes place in $\mathbb{R}^3$ with the $z$ axis as a distinguished vertical direction. The basic elements of this geometry are planes, having equation $z = f(x,y) = \alpha x + \beta y + \gamma$. The gradient vector $\nabla f = (\alpha, \beta)$ determines the plane up to translation. A plane tangent to the graph of the function $s(x,y)$ has gradient vector $\nabla s$.

There is the notion of *parallel points*: $(x,y,z) \parallel (x',y',z') \iff x = x', \; y = y'$.

*Remark:* The Maxwell paraboloid is considered the unit sphere of isotropic geometry, and the geometric quantities considered above are assigned specific meanings: The forces $\|\mathbf{e}_{ij}^*\| = w_{ij}\|\mathbf{e}_{ij}\|$ are dihedral angles of the Airy polyhedron $\Phi$, and also "lengths" of edges of $\Phi^*$. We do not use this terminology in the sequel.

**Curvatures.** Generally speaking, in the differential geometry of surfaces one considers the *Gauss map* $\sigma$ from a surface $S$ to a convex unit sphere $\Phi$ by requiring that corresponding points have parallel tangent planes. Subsequently mean curvature $H^{\mathrm{rel}}$ and Gaussian curvature $K^{\mathrm{rel}}$ *relative to* $\Phi$ are computed from the derivative $d\sigma$. Classically $\Phi$ is the ordinary unit sphere $x^2 + y^2 + z^2 = 1$, so that $\sigma$ maps each point to its unit normal vector.

In our setting, parallelity is a property of *points* rather than planes, and the Gauss map $\sigma$ goes the other way, mapping the tangent planes of the unit sphere $z = \phi(x,y)$ to the corresponding tangent plane of the surface $z = s(x,y)$. If we know which point a plane is attached to, then the Gauss map is determined by the plane's gradient. So we simply write

$$\nabla \phi \overset{\sigma}{\longmapsto} \nabla s.$$

By moving along a curve $\mathbf{u}(t) = (x(t), y(t))$ in the parameter domain we get the first variation of tangent planes: $\frac{d}{dt}\nabla\phi|_{\mathbf{u}(t)} = (\nabla^2\phi)\dot{\mathbf{u}}$. This yields the derivative $(\nabla^2\phi)\dot{\mathbf{u}} \overset{d\sigma}{\longmapsto} (\nabla^2 s)\dot{\mathbf{u}}$, for all $\dot{\mathbf{u}}$, and the matrix of $d\sigma$ is found as $(\nabla^2\phi)^{-1}(\nabla^2 s)$. By definition, curvatures of the surface $s$ relative to $\phi$ are found as

$$K_s^{\mathrm{rel}} = \det(d\sigma) = \frac{\det \nabla^2 s}{\det \nabla^2 \phi},$$

$$H_s^{\mathrm{rel}} = \tfrac{1}{2}\operatorname{tr}(d\sigma) = \tfrac{1}{2}\operatorname{tr}\left(\frac{M}{\det \nabla^2\phi}\nabla^2 s\right) = \frac{\Delta_\phi s}{2\det \nabla^2\phi}.$$

The Maxwell paraboloid $\phi_0(x,y) = \tfrac{1}{2}(x^2 + y^2)$ is the canonical unit sphere of isotropic geometry, with Hessian $E_2$. Curvatures relative to $\phi_0$ are not called "relative" and are denoted by the symbols $H, K$ instead of $H^{\mathrm{rel}}, K^{\mathrm{rel}}$. The observation

$$\Delta_\phi \phi = \operatorname{tr}(M\nabla^2\phi) = \operatorname{tr}(\widehat{\nabla^2\phi}\nabla^2\phi) = 2\det\nabla^2\phi$$

together with the formulas above implies

$$K_s = \det\nabla^2 s, \; K_\phi = \det\nabla^2\phi \implies H_s^{\mathrm{rel}} = \frac{\Delta_\phi s}{2K_\phi} = \frac{\Delta_\phi s}{\Delta_\phi \phi}.$$

**Relation to Self-supporting Surfaces.** Summarizing the formulas above, we rewrite the balance condition (1) as

$$2K_\phi H_s^{\mathrm{rel}} = \Delta_\phi s = F. \tag{4}$$

Let us draw some conclusions:

- Since $H_\phi^{\mathrm{rel}} = 1$ we see that the load $F_\phi = 2K_\phi$ is admissible for the stress surface $\phi(x,y)$, which is hereby shown as self-supporting. The quotient of loads yields $H_s^{\mathrm{rel}} = F/F_\phi$.
- If the stress surface coincides with the Maxwell paraboloid, then *constant loads characterize constant mean curvature surfaces*, because we get $K_\phi = 1$ and $H_s = F/2$.
- If $s_1, s_2$ have the same stress potential $\phi$, then $H_{s_1-s_2}^{\mathrm{rel}} = H_{s_1}^{\mathrm{rel}} - H_{s_2}^{\mathrm{rel}} = 0$, so $s_1 - s_2$ is a (relative) minimal surface.

## 2.4 Meshes in Isotropic Geometry

A general theory of curvatures of polyhedral surfaces with respect to a polyhedral unit sphere was proposed by [Pottmann et al. 2007; Bobenko et al. 2010], and its dual complement in isotropic geometry was elaborated on in [Pottmann and Liu 2007]. As illustrated by Figure 4, the mean curvature of a self-supporting surface $\mathcal{S}$ *relative* to its discrete Airy stress potential is associated with the vertices of $\mathcal{S}$. It is computed from areas and mixed areas of faces in the polar polyhedra $\mathcal{S}^*$ and $\Phi^*$:

$$H^{\mathrm{rel}}(\mathbf{v}_i) = \frac{A_i(\mathcal{S}, \Phi)}{A_i(\Phi, \Phi)}, \quad \text{where}$$

$$A_i(\mathcal{S}, \Phi) = \frac{1}{4}\sum_{k: f_k \in \text{1-ring}(\mathbf{v}_i)} \det(\mathbf{v}_k'^*, \mathbf{w}_{k+1}'^*) + \det(\mathbf{w}_k'^*, \mathbf{v}_{k+1}'^*).$$

The prime denotes the projection into the $xy$ plane, and summation is over those dual vertices which are adjacent to $\mathbf{v}_i$. Replacing $\mathbf{v}_k^*$ by $\mathbf{w}_k^*$ yields $A_i(\Phi, \Phi) = \tfrac{1}{2}\sum \det(\mathbf{w}_k'^*, \mathbf{w}_{k+1}'^*)$.
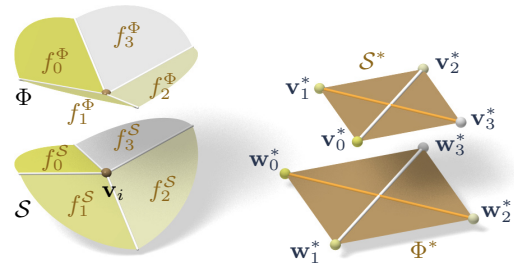


**Figure 4:** *Mean curvature of a vertex $\mathbf{v}_i$ of $\mathcal{S}$: Corresponding edges of the polar duals $\mathcal{S}^*$, $\Phi^*$ are parallel, and mean curvature according to [Pottmann et al. 2007] is computed from the vertices polar to faces adjacent to $\mathbf{v}_i$. For valence 4 vertices the case of zero mean curvature shown here is characterized by parallelity of non-corresponding diagonals of corresponding quads in $\mathcal{S}^*, \Phi^*$.*

**Proposition.** *If $\Phi$ is the Airy surface of a thrust network $\mathcal{S}$, then the mean curvature of $\mathcal{S}$ relative to $\Phi$ is computable as*

$$H^{\mathrm{rel}}(\mathbf{v}_i) = \frac{\sum_{j \sim i} w_{ij}(s_j - s_i)}{\sum_{j \sim i} w_{ij}(\phi_j - \phi_i)} = \frac{\Delta_\phi s}{\Delta_\phi \phi}\bigg|_{\mathbf{v}_i}. \tag{5}$$
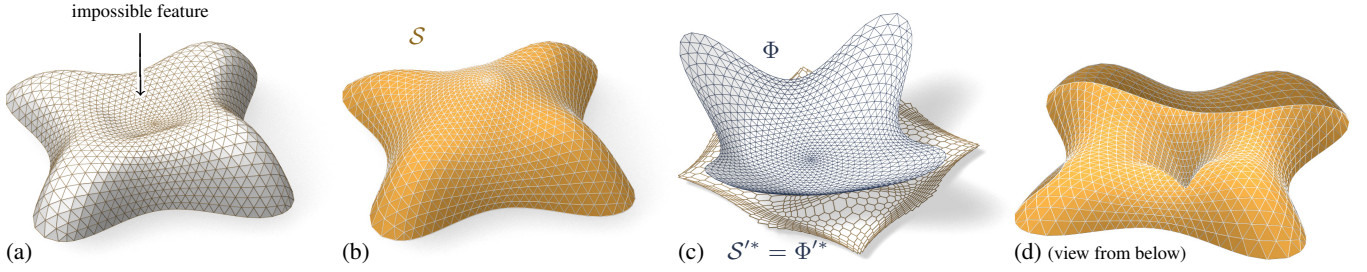
**Figure 5:** *The top of the Lilium Tower (a) cannot stand as a masonry structure, because its central part is concave. Our algorithm finds a nearby self-supporting mesh (b) without this impossible feature. (c) shows the corresponding Airy mesh $\Phi$ and reciprocal force diagram $\mathcal{S}'^*$. (d) The user can edit the original surface, such as by specifying that the center of the surface is supported by a vertical pillar, and the self-supporting network adjusts accordingly.*

*Proof.* It is sufficient to show $2A_i(\mathcal{S}, \Phi) = \sum_{j \sim i} w_{ij}(s_j - s_i)$.

For that, consider edges $\mathbf{e}'_1, \ldots, \mathbf{e}'_n$ emanating from $\mathbf{v}'_i$. The dual cycles in $\Phi^{*'}$ and $\mathcal{S}^{*'}$ without loss of generality are given by vertices $(\mathbf{v}_1^{*'}, \ldots, \mathbf{v}_n^{*'})$ and $(\mathbf{w}_1^{*'}, \ldots, \mathbf{w}_n^{*'})$, respectively. The latter has edges $\mathbf{w}_{j+1}'^* - \mathbf{w}_j'^* = w_{ij}J\mathbf{e}'_j$ (indices modulo $n$).

Without loss of generality $\mathbf{v}_i = 0$, so the vertex $\mathbf{v}_j'^*$ by construction equals the gradient of the linear function $\mathbf{x} \mapsto \langle \mathbf{v}_j'^*, \mathbf{x} \rangle$ defined by the properties $\mathbf{e}'_{j-1} \mapsto s_{j-1} - s_i$, $\mathbf{e}'_j \mapsto s_j - s_i$. Corresponding edge vectors $\mathbf{v}_{j+1}'^* - \mathbf{v}_j'^*$ and $\mathbf{w}_{j+1}'^* - \mathbf{w}_j'^*$ are parallel, because $\langle \mathbf{v}_{j+1}' - \mathbf{v}_j', \mathbf{e}'_j \rangle = (s_j - s_i) - (s_j - s_i) = 0$. Expand $2A_i(\mathcal{S}, \Phi)$:

$$\frac{1}{2}\sum \det(\mathbf{w}_j'^*, \mathbf{v}_{j+1}') + \det(\mathbf{v}_j', \mathbf{w}_{j+1}'^*)$$
$$= \frac{1}{2}\sum \det(\mathbf{w}_j'^* - \mathbf{w}_{j+1}'^*, \mathbf{v}_{j+1}') + \det(\mathbf{v}_j', \mathbf{w}_{j+1}'^* - \mathbf{w}_j'^*)$$
$$= \frac{1}{2}\sum \det(-w_{ij}J\mathbf{e}'_j, \mathbf{v}_{j+1}') + \det(\mathbf{v}_j', w_{ij}J\mathbf{e}'_j)$$
$$= \sum \det(\mathbf{v}_j', w_{ij}J\mathbf{e}'_j) = \sum w_{ij}\langle \mathbf{v}_j', \mathbf{e}'_j \rangle = \sum w_{ij}(s_j - s_i).$$

Here we have used $\det(\mathbf{a}, J\mathbf{b}) = \langle \mathbf{a}, \mathbf{b} \rangle$. $\qquad\square$

In order to discretize (4), we also need a discrete Gaussian curvature, usually defined as a quotient of areas which correspond under the Gauss mapping. We define

$$K_\Phi(\mathbf{v}_i) = \frac{A_i(\Phi, \Phi)}{A_i},$$

where $A_i$ is the Voronoi area of vertex $\mathbf{v}'_i$ in the projected mesh $\mathcal{S}'$ used in (3).

*Remark:* If the faces of the thrust network $\mathcal{S}$ are not planar, the simple trick of introducing additional edges with zero forces in them makes them planar, and the theory is applicable. In the interest of space, we refrain from elaborating further.

**Discrete Balance Equation.** The discrete version of the balance equation (4) reads as follows:

**Theorem.** *A simply-connected mesh $\mathcal{S}$ with vertices $\mathbf{v}_i = (x_i, y_i, s_i)$ can be put into static equilibrium with vertical nodal forces $A_iF_i$ if and only if there exists a combinatorially equivalent mesh $\Phi$ with planar faces and vertices $(x_i, y_i, \phi_i)$, such that curvatures of $\mathcal{S}$ relative to $\Phi$ obey*

$$2K_\Phi(\mathbf{v}_i)H^{\text{rel}}(\mathbf{v}_i) = F_i \qquad (6)$$

*at every interior vertex and every free boundary vertex $\mathbf{v}_i$. $\mathcal{S}$ can be put into compressive static equilibrium if and only if there exists a convex such $\Phi$.*

*Proof.* The relation between equilibrium forces $w_{ij}\mathbf{e}_{ij}$ in $\mathcal{S}$ and the polyhedral stress potential $\Phi$ has been discussed above, and so has the equivalence "$w_{ij} \geq 0 \iff \Phi$ convex" (see e.g. [Ash et al. 1988] for a survey of this and related results). It remains to show that Equations (2) and (6) are equivalent. This is the case because the proposition above implies $2K(\mathbf{v}_i)H^{\text{rel}}(\mathbf{v}_i) = 2\frac{A_i(\Phi, \Phi)}{A_i}\frac{A_i(\Phi, \mathcal{S})}{A_i(\Phi, \Phi)} = \frac{1}{A_i}(\sum_{j \sim i} w_{ij}(s_j - s_i)) = \frac{1}{A_i}A_iF_i.$ $\qquad\square$

### 2.5 Convergence.

When considering discrete thrust networks as discretizations of continuous self-supporting surfaces, the following question is important: For a given smooth surface $s(x, y)$ with stress potential $\phi$, does there exist a polyhedral surface $\mathcal{S}$ in equilibrium approximating $s(x, y)$, whose top view is a given planar mesh $\mathcal{S}'$? We restrict our attention to triangle meshes, where planarity of the faces of the discrete stress surface $\Phi$ is not an issue. Equivalently, we ask:

- Does $\mathcal{S}'$ have a reciprocal diagram whose corresponding Airy polyhedron $\Phi$ approximates the continuous Airy potential $\phi$? (if the surfaces involved are not simply connected, these objects are defined locally).
- Does $\mathcal{S}'$ possess a "perfect" discrete Laplace-Beltrami operator $\Delta_\phi$ in the sense of Wardetzky et al. [2007] whose weights are the edge length scalars of such a reciprocal diagram?

From [Wardetzky et al. 2007] we know that perfect Laplacians exist only on regular triangulations which are projections of convex polyhedra. On the other hand, previous sections show how to appropriately re-triangulate: Let $\Phi$ be a triangle mesh convex hull of the vertices $(x_i, y_i, \phi(x_i, y_i))$, where $(x_i, y_i)$ are vertices of $\mathcal{S}'$. Then its polar dual $\Phi^*$ projects onto a reciprocal diagram with positive edge weights, so $\Delta_\phi$ has positive weights, and the vertices $(x_i, y_i, s_i)$ of $\mathcal{S}$ can be found by solving the discrete Poisson problem $(\Delta_\phi s)_i = A_iF_i$.

We expect, but we don't prove, that the discrete $\Delta_\phi$ approximates its continuous counterpart for reasonable sampling (after all it is directly derived from $\phi(x, y)$). This implies that solving the discrete Poisson equation leads to a mesh approximating its continuous counterpart $s(x, y)$, and we have convergence as the sampling density increases. A rigorous analysis is a topic for future research.

## 3 Thrust Networks from Reference Meshes

Consider now the problem of taking a given reference mesh, say $\mathcal{R}$, and finding a combinatorially equivalent mesh $\mathcal{S}$ in static equilibrium approximating $\mathcal{R}$. The loads on $\mathcal{S}$ include user-prescribed loads as well as the dead load caused by the mesh's own weight. Conceptually, finding $\mathcal{S}$ amounts to minimizing some formulation
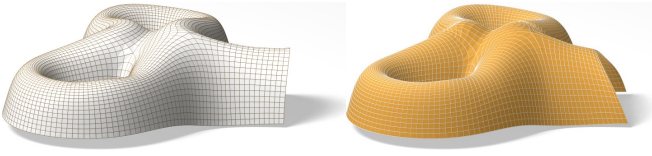
**Figure 6:** *A freeform surface (left) needs adjustments around the entrance arch and between the two pillars in order to be self-supporting; our algorithm finds the nearby surface in equilibrium (right) that incorporates these changes.*

| Fig. | Vertices | Edges | Time (s) | Iterations | Max. Rel. Error |
|---|---|---|---|---|---|
| 5b | 1201 | 3504 | 21.6 | 9 | $4.2 \times 10^{-5}$ |
| 5d | 1200 | 3500 | 26.5 | 10 | $8.5 \times 10^{-5}$ |
| 6 | 1535 | 2976 | 17.0 | 21 | $2.7 \times 10^{-5}$ |
| 8 | 752 | 2165 | 8.0 | 9 | $5.8 \times 10^{-5}$ |
| 11 | 2358 | 4302 | 19.5 | 9 | $3.0 \times 10^{-4}$ |
| 16 | 527 | 998 | 5.7 | 25 | $2.4 \times 10^{-5}$ |

**Table 1:** *Numerical details about our examples. We show the clock time needed by an Intel Xeon 2.3GHz desktop PC with 4 GB of RAM to find a self-supporting thrust network and associated stress surface from the example's reference mesh; we also give the number of outer iterations of the four steps in (§3). The maximum relative error is the dimensionless quantity $\max_i \|A_i F_i \binom{0}{1} - \sum_{j \sim i} w_{ij}(\mathbf{v}_j - \mathbf{v}_i)\|/A_i F_i$ (the maximum is taken over interior vertices $\mathbf{v}_i$).*

of distance between $\mathcal{R}$ and $\mathcal{S}$, subject to constraints (2), (3), and $w_{ij} \geq 0$. For any choice of distance this minimization will be a nonlinear, non-convex, inequality-constrained variational problem. Our experience with black-box solvers [Wächter and Biegler 2006] is that they perform well for surfaces without complex geometry or for polishing reference meshes close to self-supporting, but fail to converge in reasonable time for more complicated shapes such as the one of Fig. 1, left. We therefore propose the following specialized, staggered linearization for solving the optimization problem:

0. Start with an initial guess $\mathcal{S} = \mathcal{R}$.
1. Estimate the self-load on the vertices of $\mathcal{S}$, using their current positions.
2. Fixing $\mathcal{S}$, locally fit an associated stress surface $\Phi$.
3. Alter positions $\mathbf{v}_i$ to improve the fit.
4. Repeat from Step 1 until convergence.

*Remark:* This staggered approach shares several advantages of solving the full nonlinear problem: a nearby self-supporting surface is found given only a suggested reference shape, without needing to single one of the many possible top view reciprocal diagrams or needing to specify boundary tractions – these are found automatically during optimization. Although providing an initial top view graph with good combinatorics remains important, by not fixing the top view our approach allows the thrust network to slide both vertically and tangentially to the ground, essential to finding faithful thrust networks for surfaces with free boundary conditions.

**Step 1: Estimating Self-Load.** The dead load due to the surface's own weight depends not only on the top view of $\mathcal{S}$, but also on the surface area of its faces. To avoid adding nonlinearity to the algorithm, we estimate the load coefficients $F_i$ at the beginning of each iteration, and assume they remain constant until the next iteration. We estimate the load $A_i F_i$ associated with each vertex by calculating its Voronoi surface area on each of its incident faces (note that this surface area is distinct from $A_i$, the vertex's Voronoi area on the top view), and then multiplying by a user-specified surface density $\rho$.

**Step 2: Fit a Stress Surface.** In this step, we fix $\mathcal{S}$ and try to fit a stress surface $\Phi$ subordinate to the top view $\mathcal{S}'$ of the primal mesh. We do so by searching for dihedral angles between the faces of $\Phi$ which minimize, in the least-squares sense, the error in force equilibrium (6) and local integrability of $\Phi$. Doing so is equivalent to minimizing the squared residuals of Equations (3) and (2), with the positions held fixed. We define the *equilibrium energy*

$$E = \sum_i \left\| \begin{pmatrix} 0 \\ 0 \\ A_i F_i \end{pmatrix} - \sum_{j \sim i} w_{ij}(\mathbf{v}_j - \mathbf{v}_i) \right\|^2, \qquad (7)$$

where $i$ runs through interior and free boundary vertices, and solve

$$\min_{w_{ij}} E, \quad \text{s.t. } 0 \leq w_{ij} \leq w_{\max}. \qquad (8)$$

Here $w_{\max}$ is an optional maximum weight we are willing to assign (to limit the amount of stress in the surface). This convex, sparse, box-constrained least-squares problem [Friedlander 2007] always has a solution. If the objective is 0 at this solution, $\mathcal{S}$ is self-supporting – we are done. Otherwise, $\mathcal{S}$ is not self-supporting and its vertices must be moved.

**Step 3: Alter Positions.** In the previous step we fit as best as possible a stress surface $\Phi$ to $\mathcal{S}$. There are two possible kinds of error with this fit: the faces around a vertex (equivalently, the reciprocal diagram) might not close up; and the resulting stress forces might not be exactly in equilibrium with the loads. These errors can be decreased by modifying the top view and heights of $\mathcal{S}$, respectively. It is possible to simply solve for new vertex positions that put $\mathcal{S}$ in static equilibrium, since Equations (2) and (3) with $w_{ij}$ fixed form a square linear system that is typically nonsingular.

While this approach would yield a self-supporting $\mathcal{S}$, this mesh is often far from the reference mesh $\mathcal{R}$, since any local errors in the stress surface from Step 2 amplify into global errors in $\mathcal{S}$. We propose instead to look for new positions that decrease the imbalance in the stresses and loads, while also penalizing drift away from the reference mesh:

$$\min_{\mathbf{v}} E + \alpha \sum_i \langle \mathbf{n}_i, \mathbf{v}_i - \mathbf{v}_i^0 \rangle^2 + \beta \|\mathbf{v} - \mathbf{v}_P^0\|^2,$$

where $\mathbf{v}_i^0$ is the position of the $i$-th vertex at the start of this step of the optimization, $\mathbf{n}_i$ is the starting vertex normal (computed as the average of the incident face normals), $\mathbf{v}_P^0$ is the projection of $\mathbf{v}^0$ onto the reference mesh, and $\alpha > \beta$ are penalty coefficients that are decreased proportionally to the decrease in $E$ at every iteration of Steps 1–3. $\alpha = 1$ and $\beta = 0.1$ worked well as initial values of these parameters for the examples shown in this paper. The second term allows $\mathcal{S}$ to slide over itself (if doing so improves equilibrium) but penalizes drift in the normal direction. The third term, weaker than the second, regularizes the optimization by preventing large drift away from the reference surface or excessive tangential sliding.

**Implementation Details.** Solving the weighted least-squares problem of Step 3 amounts to solving a sparse, symmetric linear system. While the MINRES algorithm [Paige and Saunders 1975] is likely the most robust algorithm for solving this system, in practice we have observed that the method of conjugate gradients works well despite the potential ill-conditioning of the objective matrix.

**Limitations.** This algorithm is not guaranteed to always converge; this fact is not surprising from the physics of the problem
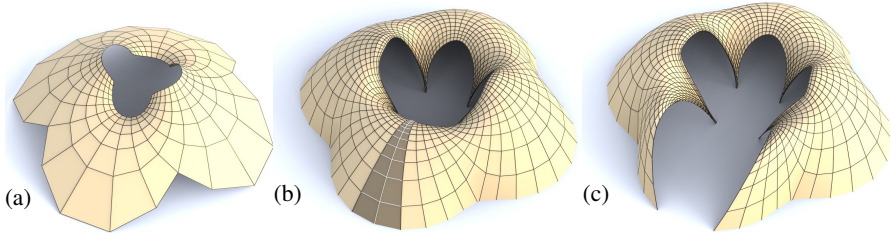
**Figure 7:** *Interactive Edits. (a) shows a self-supporting thrust network – in fact it is a Koebe mesh as mentioned in §5. In (b) boundary conditions are defined and pillars have been added. Cutting along the highlighted edge and optimizing for the self-supporting property results in the mesh shown in (c).*
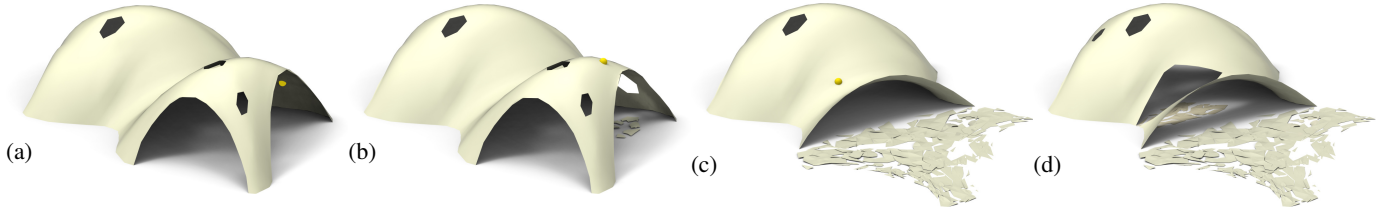


**Figure 8:** *Destruction sequence. We simulate removing small parts of masonry (their location is shown by a yellow ball) and the falling off of further pieces which are no longer supported after removal. For this example, removing a certain small number of single bricks does not affect stability (a,b). Removal of material at a certain point (yellow ball in (b)) will cause a greater part of the structure to collapse, as seen in (c). (d) shows the result after one more removal (all images show the respective thrust networks, not the reference surface).*

(if the boundary of the reference mesh encloses too large of a region, $w_{\max}$ is set too low, and the density of the surface too high, a thrust network in equilibrium simply does not exist – the vault is too ambitious and cannot be built to stand; pillars are needed.)

We can, however, make a few remarks. Only Step 1 can increase the equilibrium energy $E$ of Equation (7). Step 2 always decreases it, and Step 3 does as well as $\beta \to 0$. Moreover, as $\alpha \to 0$ and $\beta \to 0$, Step 3 approaches a linear system with as many equations as unknowns; if this system has full rank, its solution sets $E = 0$. These facts suggest that the algorithm should generally converge to a thrust network in equilibrium, provided that Step 1 does not increase the loads by too much at every iteration, and this is indeed what we observe in practice. One case where this assumption is guaranteed to hold is if the thickness of the surface is allowed to freely vary, so that it can be chosen so that the surface has uniform density over the top view.

We have observed several situations where our algorithm has difficulty converging to a high-quality solution, even though the underlying optimization problem is feasible:

- Vertices with high valence (such as can occur at irregular vertices of triangle meshes) often become local maxima ("bumps") after optimization. In the worst case, the algorithm can stall at $E > 0$ due to the linear system in Step 3 becoming singular and infeasible. This failure occurs, for instance, when an interior vertex has height $z_i$ lower than all of its neighbors, and Step 2 assigns all incident edges to that vertex a weight of zero: clearly no amount of moving the vertex or its neighbors can bring the vertex into equilibrium. We avoid such degenerate configurations by bounding weights slightly away from zero in (8), trading increased robustness for slight smoothing of the resulting surface. We also haven't noticed these artifacts in lower-valence meshes such as quad meshes.

- The algorithm does not usually converge if the reference mesh has a self-intersecting top view (i.e., isn't a height field), although it can occasionally correct slight overhangs (by deforming the top view so that the network mesh is a height field).

- The algorithm may not converge if the deformation needed to

make the refence mesh self-supporting is too large. Specifying a reference mesh insufficiently supported by fixed boundary vertices is the most common such situation – for instance, marking the bases of the pillars in Fig. 7 as free instead of fixed boundaries causes our algorithm to fail, even though a (drastic) self-supporting deformation of that surface does exist.

# 4 Results

**Interactive Design of Self-Supporting Surfaces.** The optimization algorithm described in the previous section forms the basis of an interactive design tool for self-supporting surfaces. Users manipulate a mesh representing a reference surface, and the computer searches for a nearby thrust network in equilibrium (see e.g. Figure 7). Features of the design tool include:

- Handle-based 3D editing of the reference mesh using Laplacian coordinates [Lipman et al. 2004; Sorkine et al. 2003] to extrude vaults, insert pillars, and apply other deformations to the reference mesh. Handle-based adjustments of the heights, keeping the top view fixed, and deformation of the top view, keeping the heights fixed, are also supported. The thrust network adjusts interactively to fit the deformed positions, giving the usual visual feedback about the effects of edits on whether or not the surface can stand.
- Specification of boundary conditions. Points of contact between the reference surface and the ground or environment are specified by "pinning" vertices of the surface, specifying that the thrust network must coincide with the reference mesh at this point, and relaxing the condition that forces must be in equilibrium there.
- Interactive adjustment of surface density, external loads, and maximum permissible stress per edge, with visual feedback of how these parameters affect the fitted thrust network.
- Upsampling of the thrust network through Catmull-Clark subdivision and polishing of the resulting refined thrust network using optimization (§3).
- Visualization of the stress surface dual to the thrust network and corresponding reciprocal diagram.

**Figure 9:** *Stability Test. Left: Coloring and cross-section of edges visualize the magnitude of forces in a thrust network which is in equilibrium with this dome's dead load. Right: When an additional load is applied, there exists a corresponding compressive thrust network which is still contained in the masonry hull of the original dome. This implies stability of the dome under that load.*
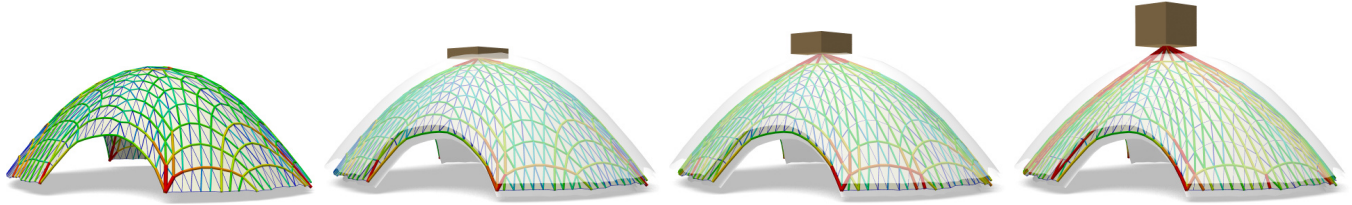
shell thickness 0.1 m, $\rho = 2,500 \, \mathrm{kg/m^3}$

11,000 kg

14 m



**Figure 10:** *Stability test similar to Figure 9, but with a shell thickness of 1 m, in order to better visualize the way the thrust network starts to leave the masonry hull as the load increases. Additional loads are 0 kg, 5,000 kg, 10,000 kg, and 20,000 kg, resp., from left to right.*

**Examples.** *Top of the Lilium Tower:* Consider the top portion of the steel-glass exterior surface of the Lilium Tower (being built in Warszaw, see Fig. 5). What is if we had wanted to build this surface out of masonry instead? This surface contains a concave part with local minimum in its interior and so cannot possibly be self-supporting without modification. Given this surface as a reference mesh, our algorithm constructs a nearby thrust network in equilibrium without the impossible feature. The user can then explore how editing the reference mesh – adding a pillar, for example – affects the thrust network and its deviation from the reference surface.

*Example: Freeform Structure with Two Pillars.* Suppose an architect's experience and intuition has permitted the design of a nearly self-supporting freeform surface (Figure 6). Our algorithm reveals those edits needed to make the structure sound – principally around the entrance arch, and the area between the two pillars.
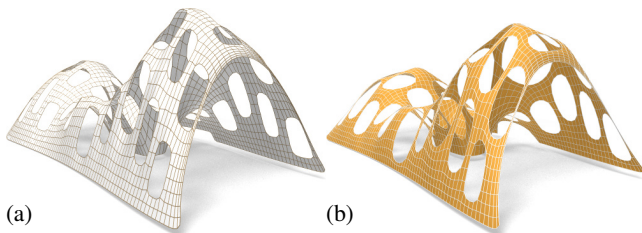


(a)                                    (b)

**Figure 11:** *A mesh with holes (a) requires large deformations to both the top view and heights to render it self-supporting (b)*

*Example: Interactive Editing.* Figure 7 shows an example of the design and optimization workflow. Starting with a mesh, we first add pillars in the center and clean up the outer boundary (by fixing it to the floor). A subsequent cut needs a further round of optimization. This surface is neither convex nor simply connected, and exhibits a mix of boundary conditions, none of which cause our algorithm any difficulty; it always finds a self-supporting thrust network near the designed reference mesh. The user is free to make edits to the reference mesh, and the thrust network adapts to these edits, providing the user feedback on whether these designs are physically realizable *[we refer to the accompanying video for interactive building and editing of freeform self-supporting shapes].*

*Example: Destruction Sequence.* In Figure 8 we simulate removing parts of masonry and the falling off of further pieces which are no longer supported after removal. This is done by deleting the 1-neighborhood of a vertex and solving for a new thrust network in

compressive equilibrium close to the original reference surface. We delete those parts of the network which deviate too much and are no longer contained in the masonry hull, and iterate.

*Example: Swiss Cheese.* Cutting holes in a self-supporting surface interrupts force flow lines and causes dramatic global changes to the surface stresses, often to the point that the surface is no longer in equilibrium. Whether a given surface with many such holes can stand is far from obvious. Figure 11a shows such an implausible and unstable surface; our optimization finds a nearby, equally implausible but stable surface without difficulty (Figs. 1, left and 11b).

*Example: Stability Test:* See Figures 9, 10 for a series of images which visualize the effect of additional loads on a thrust network.

*Example: Structural Glass.* See Figure 16 for details on a self-supporting surface which is realized not as masonry, but as a steel/glass construction with glass as a structural element.

## 5 Special Self-Supporting Surfaces

**PQ Meshes.** Meshes with *planar* faces are of particular interest in architecture, so in this section we discuss how to remesh a given thrust network in equilibrium such that it becomes a quad mesh with planar faces (again in equilibrium). If this mesh is realized as a steel-glass construction, it is self-supporting in its beams alone, with no forces exerted on the glass (this is the usual manner of using glass). The beams constitute a self-supporting structure which is in perfect force equilibrium (without moments in the nodes) if only the deadload is applied. (In such constructions, the restriction that the internal forces are compressive does not apply.)
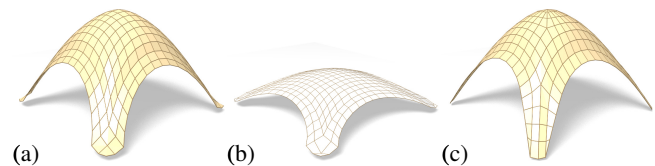


(a)                    (b)                    (c)

**Figure 12:** *Directly enforcing planarity of the faces of even a very simple self-supporting quad-mesh vault (a) results in a surface far removed from the original design (b). Starting instead from a remeshing of the surface with edges following relative principal curvature directions yields a self-supporting, PQ mesh far more faithful to the original (c).*

Taking an arbitrary non-planar quad mesh and attempting naive, si-

**Figure 13:** *Planar quad remeshing of the surface of Fig. 5. (a) Relative principal directions, found from eigenvectors of $(\nabla^2\phi)^{-1}\nabla^2 s$. (b) Quad mesh guided by principal directions is almost planar and almost self-supporting. (c) Small changes achieve both properties.*
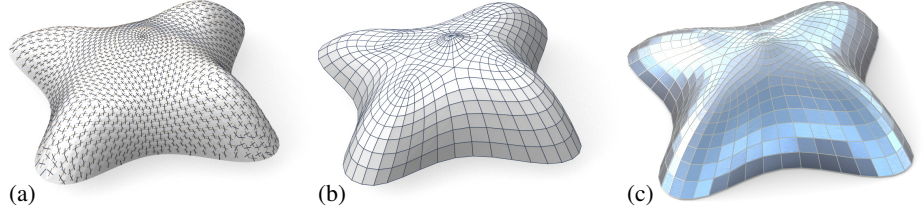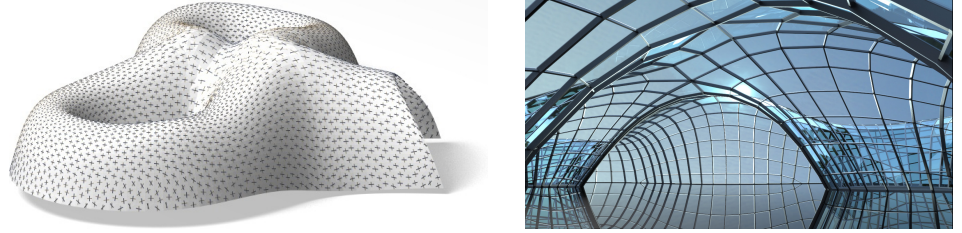
(a)  (b)  (c)



**Figure 14:** *Planar quad remeshing of the surface of Figure 6. Left: Relative principal directions. Right: The result of optimization is a self-supporting PQ mesh, which guides a moment-free steel/glass construction (interior view, see also Fig. 1).*

multaneous enforcement of planarity and static equilibrium – either by staggering a planarity optimization step every outer iteration, or adding a planarity penalty term to the position update – does not yield good results, as shown in Figure 12. Indeed, as we will see later in this section, such a planar perturbation of a thrust network is not expected to generally exist.

Consider a planar quad mesh $\mathcal{S}$ with vertices $\mathbf{v}_{ij} = (x_{ij}, y_{ij}, s_{ij})$ which approximates a given continuous surface $s(x, y)$. It is known that $\mathcal{S}$ must approximately follow a network of conjugate curves in the surface (see e.g. [Liu et al. 2006]). We can derive this condition in an elementary way as follows: Using a Taylor expansion, we compute the volume of the convex hull of the quadrilateral $\mathbf{v}_{ij}$, $\mathbf{v}_{i+1,j}$, $\mathbf{v}_{i+1,j+1}$, $\mathbf{v}_{i,j+1}$, assuming the vertices lie exactly on the surface $s(x, y)$. This results in

$$\mathrm{vol} = \tfrac{1}{6}\det(\mathbf{a}_1, \mathbf{a}_2) \cdot \left((\mathbf{a}_1)^T \nabla^2 s\, \mathbf{a}_2\right) + \cdots,$$
$$\text{where } \mathbf{a}_1 = \begin{pmatrix} x_{i+1,j}-x_{ij} \\ y_{i+1,j}-y_{ij} \end{pmatrix}, \quad \mathbf{a}_2 = \begin{pmatrix} x_{i,j+1}-x_{ij} \\ y_{i,j+1}-y_{ij} \end{pmatrix},$$

and the dots indicate higher order terms. We see that planarity requires $(\mathbf{a}_1)^T \nabla^2 s\, \mathbf{a}_2 = 0$. In addition to the mesh $\mathcal{S}$ approximating the surface $s(x, y)$, the corresponding polyhedral Airy surface $\Phi$ must approximate $\phi(x, y)$; thus we get the conditions

$$(\mathbf{a}_1)^T \nabla^2 s\, \mathbf{a}_2 = (\mathbf{a}_1)^T \nabla^2 \phi\, \mathbf{a}_2 = 0.$$

$\mathbf{a}_1, \mathbf{a}_2$ are therefore eigenvectors of $(\nabla^2\phi)^{-1}\nabla^2 s$. In view of §2.3, $\mathbf{a}_1, \mathbf{a}_2$ indicate the principal directions of the surface $s(x, y)$ relative to $\phi(x, y)$.

In the discrete case, where $s, \phi$ are not given as continuous surfaces, but are represented by a mesh in equilibrium and its Airy mesh, we use the techniques of Schiftner [2007] and Cohen-Steiner and Morvan [2003] to approximate the Hessians $\nabla^2 s$, $\nabla^2 \phi$, compute principal directions as eigenvectors of $(\nabla^2\phi)^{-1}\nabla^2 s$, and subsequently find meshes $\mathcal{S}, \Phi$ approximating $s, \phi$ which follow those directions. Global optimization can now polish $\mathcal{S}, \Phi$ to a valid thrust network with discrete stress potential, where before it failed: we do so by taking the planarity energy $\sum_f (2\pi - \theta_f)^2$, where the sum runs over faces and $\theta_f$ is the sum of the interior angles of face $f$, linearizing it at every iteration, and adding it to the objective function of the position update (Step 3). Convexity of $\Phi$ ensures that $\mathcal{S}$ is self-supporting.

Note that for each $\Phi$, the relative principal curvature directions give the *unique* curve network along which a planar quad discretization

of a self-supporting surface is possible. Other networks won't work (see Figure 12). Figures 13 and 14 further illustrate the result of applying this procedure to self-supporting surfaces.

*Remark:* When remeshing a given shape by planar quad meshes, we know that the circular and conical properties require that the mesh follows the ordinary, Euclidean principal curvature directions [Liu et al. 2006]. It is remarkable that the self-supporting property in a similar manner requires us to follow certain *relative* principal directions. Practitioners' observations regarding the beneficial statics properties of principal directions can be explained by this analogy, because the relative principal directions are close to the Euclidean ones, if the stress distribution is uniform and $\|\nabla s\|$ is small.

**Koenigs Meshes.** Given a self-supporting thrust network $\mathcal{S}$ with stress surface $\Phi$, we ask the question: Which vertical perturbation $\mathcal{S} + \mathcal{R}$ is self-supporting, with the same loads as $\mathcal{S}$? As to notation, all involved meshes $\mathcal{S}, \mathcal{R}, \Phi$ have the same top view, and arithmetic operations refer to the respective $z$ coordinates $s_i, r_i, \phi_i$ of vertices.

The condition of equal loads then is expressed as $\Delta_\phi(s+r) = \Delta_\phi s$ in terms of Laplacians or as $H^{\mathrm{rel}}_{\mathcal{S}} = H^{\mathrm{rel}}_{\mathcal{S}+\mathcal{R}}$ in terms of mean curvature, and is equivalent to $\Delta_\phi r = 0$, i.e., $H^{\mathrm{rel}}_{\mathcal{R}} = 0$. So $\mathcal{R}$ is a *minimal surface* relative to $\Phi$. While in the triangle mesh case there are enough degrees of freedom for nontrivial solutions, the case of planar quad meshes is more intricate: Polar polyhedra $\mathcal{R}^*, \Phi^*$ have to be Christoffel duals of each other [Pottmann and Liu 2007], as illustrated by Figure 4. Unfortunately not all quad meshes have such a dual; the condition is that the mesh is *Koenigs*, i.e., the derived mesh formed by the intersection points of diagonals of faces again has planar faces [Bobenko and Suris 2008].

**Koebe meshes.** An interesting special case occurs if $\Phi$ is a *Koebe mesh* of isotropic geometry, i.e., a PQ mesh whose edges touch the Maxwell paraboloid. Since $\Phi$ approximates the Maxwell paraboloid, we get $2K(\mathbf{v}_i)H^{\mathrm{rel}}(\mathbf{v}_i) \approx 1$ and $\Phi$ consequently is self-supporting for unit load. Applying the Christoffel dual construction described above yields a minimal mesh $\mathcal{R}$, and meshes $\Phi + \alpha\mathcal{R}$ which are self-supporting for unit load (see Figure 15).

## 6 Conclusion and Future Work

**Conclusion.** This paper builds on relations between statics and geometry, some of which have been known for a long time, and
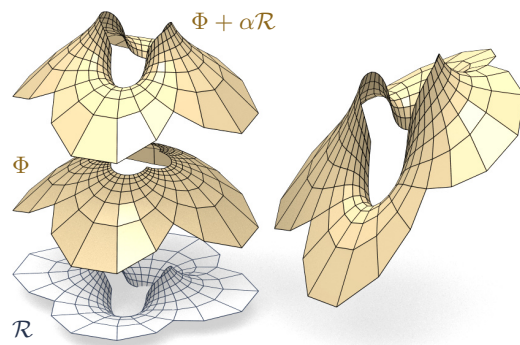
**Figure 15:** *Left: A "Koebe" mesh $\Phi$ is self-supporting for unit dead load. An family of self-supporting meshes with the same top view is defined by $\mathcal{S}_\alpha = \Phi + \alpha\mathcal{R}$, where $\mathcal{R}$ is chosen as $\Phi$'s Christoffel-dual. The right hand image shows a different example of the same connectivity.*

connects them with newer methods of discrete differential geometry, such as discrete Laplace operators and curvatures of polyhedral surfaces. We were able to find efficient ways of modeling self-supporting freeform shapes, and provide architects and engineers with an interactive tool for evaluating the statics of freeform geometries. The self-supporting property of a shape is directly relevant for freeform masonry. The actual thrust networks we use for computation are relevant e.g. for steel constructions, where equilibrium of deadload forces implies absence of moments. This theory and accompanying algorithms thus constitute a new contribution to architectural geometry, connecting statics and geometric design.

**Future Work.** There are several directions of future research. One is to incorporate non-manifold meshes, which occur naturally when e.g. supporting walls are introduced. It is also obvious that non-vertical loads, e.g. wind load, play a role. The surfaces produced by our algorithm are the solutions of discrete elliptic boundary value problems and so tend to be smooth; another avenue for future work is modification of the discretization to allow for self-supporting surfaces with sharp features. There are also some directions to pursue in improving the algorithms, for instance adaptive remeshing in problem areas. Probably the interesting connections between stat-

ics and geometry are not yet exhausted: on the one hand we expect that interesting new geometry arises from questions of statics, on the other hand we would like to propose the *geometrization* of problems as a general solution paradigm.

## References

ANDREU, A., GIL, L., AND ROCA, P. 2007. Computational analysis of masonry structures with a funicular model. *J. Engrg. Mechanics 133*, 473-480.

ASH, P., BOLKER, E., CRAPO, H., AND WHITELEY, W. 1988. Convex polyhedra, Dirichlet tessellations, and spider webs. In *Shaping space (Northampton 1984)*. Birkhäuser, 231–250.

BARNES, M. R. 2009. Form finding and analysis of tension structures by dynamic relaxation. *Int. J. Space Struct. 14*, 2, 89–104.

BLOCK, P., AND LACHAUER, L. 2011. Closest-fit, compression-only solutions for free form shells. In *IABSE — IASS 2011 London Symposium*, Int. Ass. Shell Spatial Structures. [electronic].

BLOCK, P., AND OCHSENDORF, J. 2007. Thrust network analysis: A new methodology for three-dimensional equilibrium. *J. Int. Assoc. Shell and Spatial Structures 48*, 3, 167–173.

BLOCK, P. 2009. *Thrust Network Analysis: Exploring Three-dimensional Equilibrium*. PhD thesis, Massachusetts Institute of Technology.

BLOCK, P., 2011. Project webpage at *http://block.arch.ethz.ch/projects/freeform-catalan-thin-tile-vaulting*.

BOBENKO, A., AND SURIS, YU. 2008. *Discrete differential geometry: Integrable Structure*. No. 98 in Graduate Studies in Math. American Math. Soc.

BOBENKO, A., POTTMANN, H., AND WALLNER, J. 2010. A curvature theory for discrete surfaces based on mesh parallelity. *Math. Annalen 348*, 1–24.

COHEN-STEINER, D., AND MORVAN, J.-M. 2003. Restricted Delaunay triangulations and normal cycle. In *Proc. 19th Symp. Computational Geometry*, ACM, 312–321.

DAVIS, L., RIPPMANN, M., PAWLOFSKY, T., AND BLOCK, P. 2011. Efficient and expressive thin-tile vaulting using cardboard formwork. In *IABSE — IASS 2011 London Symposium*, Int. Ass. Shell Spatial Structures. [electronic].

FRATERNALI, F., ANGELILLO, M., AND FORTUNATO, A. 2002. A lumped stress method for plane elastic problems and the discrete-continuum approximation. *Int. J. Solids Struct. 39*, 6211–6240.

FRATERNALI, F. 2010. A thrust network approach to the equilibrium problem of unreinforced masonry vaults via polyhedral stress functions. *Mechanics Res. Comm. 37*, 2, 198 – 204.

FRIEDLANDER, M. P., 2007. BCLS: Bound constrained least squares. *http://www.cs.ubc.ca/~mpf/bcls*.

GIAQUINTA, M., AND GIUSTI, E. 1985. Researches on the equilibrium of masonry structures. *Archive for Rational Mechanics and Analysis 88*, 4, 359–392.

GREEN, A., AND ZERNA, W. 2002. *Theoretical Elasticity*. Dover. Reprint of the 1968 edition.

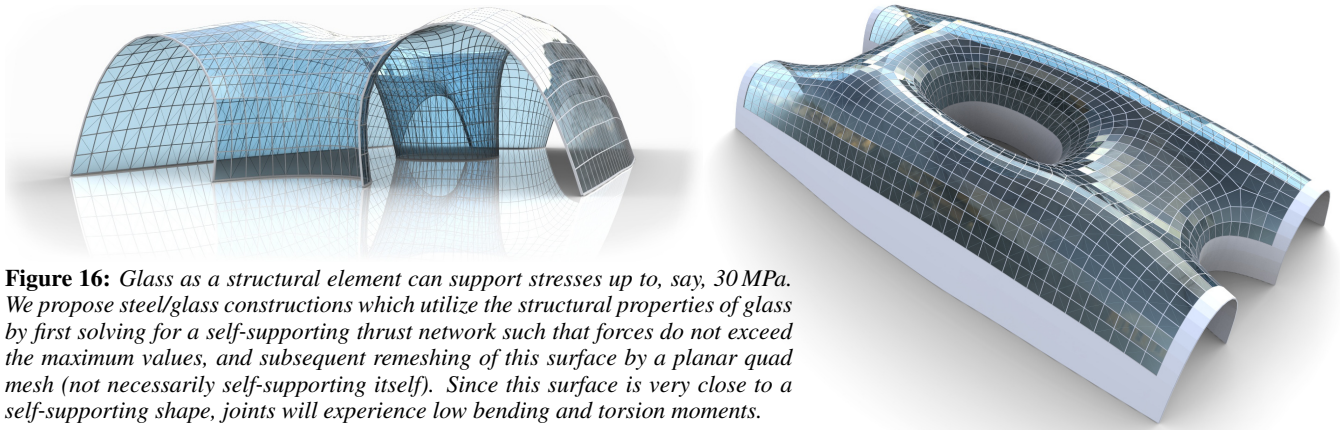GRÜNDIG, L., MONCRIEFF, E., SINGER, P., AND STRÖBEL, D. 2000. A history of the principal developments and applications

**Figure 16:** *Glass as a structural element can support stresses up to, say, 30 MPa. We propose steel/glass constructions which utilize the structural properties of glass by first solving for a self-supporting thrust network such that forces do not exceed the maximum values, and subsequent remeshing of this surface by a planar quad mesh (not necessarily self-supporting itself). Since this surface is very close to a self-supporting shape, joints will experience low bending and torsion moments.*

of the force density method in Germany 1970–1999. In *4th Int. Coll. Computation of Shell & Spatial Structures*.

HEYMAN, J. 1966. The stone skeleton. *Int. J. Solids Structures 2*, 249–279.

HEYMAN, J. 1995. *The Stone Skeleton: Structural Engineering of Masonry Architecture*. Cambridge University Press.

HEYMAN, J. 1998. *Structural Analysis: A Historical Approach*. Cambridge University Press.

KILIAN, A., AND OCHSENDORF, J. 2005. Particle-spring systems for structural form finding. *J. Int. Assoc. Shell and Spatial Structures 46*, 77–84.

KOTNIK, T., AND WEINSTOCK, M. 2012. Material, form and force. *Architectural Design 82*, 104–111.

LINKWITZ, K., AND SCHEK, H.-J. 1971. Einige Bemerkungen zur Berechnung von vorgespannten Seilnetzkonstruktionen. *Ingenieur-Archiv 40*, 145–158.

LIPMAN, Y., SORKINE, O., COHEN-OR, D., LEVIN, D., ROSSI, C., AND SEIDEL, H. 2004. Differential coordinates for interactive mesh editing. In *Shape Modeling Applications, 2004. Proceedings*. IEEE, 181–190.

LIU, Y., POTTMANN, H., WALLNER, J., YANG, Y.-L., AND WANG, W. 2006. Geometric modeling with conical meshes and developable surfaces. *ACM Trans. Graphics 25*, 3, 681–689. Proc. SIGGRAPH.

LIVESLEY, R. K. 1992. A computational model for the limit analysis of three-dimensional masonry structures. *Meccanica 27*, 161–172.

O'DWYER, D. 1998. Funicular analysis of masonry vaults. *Computers and Structures 73*, 187–197.

PAIGE, C. C., AND SAUNDERS, M. A. 1975. Solution of sparse indefinite systems of linear equations. *SIAM J. Num. Analysis 12*, 617–629.

POTTMANN, H., AND LIU, Y. 2007. Discrete surfaces in isotropic geometry. In *Mathematics of Surfaces XII*, M. Sabin and J. Winkler, Eds. Springer, 341–363.

POTTMANN, H., LIU, Y., WALLNER, J., BOBENKO, A., AND WANG, W. 2007. Geometry of multi-layer freeform structures for architecture. *ACM Trans. Graphics 26*, 3, #65,1–11. Proc. SIGGRAPH.

SCHIFTNER, A., AND BALZER, J. 2010. Statics-sensitive layout of planar quadrilateral meshes. In *Advances in Architectural Geometry 2010*, C. Ceccato et al., Eds. Springer, Vienna, 221–236.

SCHIFTNER, A. 2007. *Planar quad meshes from relative principal curvature lines*. Master's thesis, TU Wien. *http://dmg.tuwien.ac.at/aschiftner/doc/diplomarbeit.pdf*.

SORKINE, O., COHEN-OR, D., AND TOLEDO, S. 2003. High-pass quantization for mesh encoding. In *Symposium Geometry processing*, L. Kobbelt, P. Schröder, and H. Hoppe, Eds. Eurographics Assoc., 42–51.

VAN MELE, T., AND BLOCK, P. 2011. A novel form finding method for fabric formwork for concrete shells. *J. Int. Assoc. Shell and Spatial Structures 52*, 217–224.

WÄCHTER, A., AND BIEGLER, L. T. 2006. On the implementation of a primal-dual interior point filter line search algorithm for large-scale nonlinear programming. *Math. Progr. 106*, 25–57.

WARDETZKY, M., MATHUR, S., KÄLBERER, F., AND GRINSPUN, E. 2007. Discrete Laplace operators: No free lunch. In *Symposium on Geometry Processing*, A. Belyaev and M. Garland, Eds. Eurographics Assoc., 33–37.

WHITING, E., OCHSENDORF, J., AND DURAND, F. 2009. Procedural modeling of structurally-sound masonry buildings. *ACM Trans. Graphics 28*, 5, #112,1–9. Proc. SIGGRAPH Asia.